Flexural strengthening of RC beams using textile reinforced mortar – Experimental and numerical study

Hussein M. Elsanadedy [*,1], Tarek H. Almusallam, Saleh H. Alsayed, Yousef A. Al-Salloum

Specialty Units for Safety & Preservation of Structures, Department of Civil Engineering, King Saud University, P.O. Box 800, Riyadh 11421, Saudi Arabia

ARTICLE INFO

ABSTRACT

In this paper, the effectiveness of textile reinforced mortars (TRMs), as a means of increasing the flexural capacity of reinforced concrete (RC) beams, is experimentally and numerically investigated. A new type of textile (basalt-based textile) was used as strengthening material. The studied parameters included type of mortar, number of TRM layers and type of strengthening material: TRM versus carbon fiber-reinforced polymer (CFRP) composites. A total of six beams were tested under four-point bending till failure. Two beams were used as control specimens. Three beams were externally upgraded by TRM sheets for enhancing their flexural capacity; and one beam was strengthened with CFRP laminates for comparison with its TRM counterpart. Besides the experimental program, a numerical investigation utilizing nonlinear finite element (FE) analysis was carried out using LS-DYNA software. In addition to the six beams tested in this study, another three beams were collected from the literature for the purpose of finite element validation. A comparison was made between the experimental and numerical results and good agreement was obtained. Based on the validation of FE results, the numerical analysis was extended to include additional cases to study the flexural enhancement of RC beams using more TRM layers with different end anchorages.

© 2012 Elsevier Ltd. All rights reserved.

1. Introduction

There is an increasing demand in the past years for rehabilitating existing structures due to deterioration and/or the introduction of more strict design requirements. One of the most common strengthening techniques for reinforced concrete members involves the use of fiber reinforced polymer (FRP) composites. The use of FRP has acquired increasing popularity in the civil engineering community, due to the favorable properties possessed by these materials, namely: extremely high strength-to-weight ratio, corrosion resistance, ease and speed of application and minimal change in the geometry [1]. Despite all these advantages, the FRP strengthening technique has a few disadvantages, which are attributed to the resins used to bind or impregnate the fibers [2–5]. These drawbacks may include: (a) de-bonding of FRP from the concrete substrate; (b) poor behavior of epoxy resins at temperatures above the glass transition temperature; (c) relatively high cost of epoxies; (d) inability to apply FRP on wet surfaces or at low temperatures; (e) lack of vapor permeability, which may cause damage to the concrete structure; (f) incompatibility of epoxy resins and sub-strate materials; (g) difficulty to conduct post-earthquake assessment of the damage suffered by the reinforced concrete behind (undamaged) FRP jackets. One possible solution to the above problems would be the replacement of organic by inorganic binders, e.g. cement-based mortars, leading to the replacement of FRP with fiber reinforced mortars (FRMs). Due to the granularity of the mortar, penetration and impregnation of fiber sheets is very difficult to achieve; also, unlike resins, mortars cannot wet individual fibers.
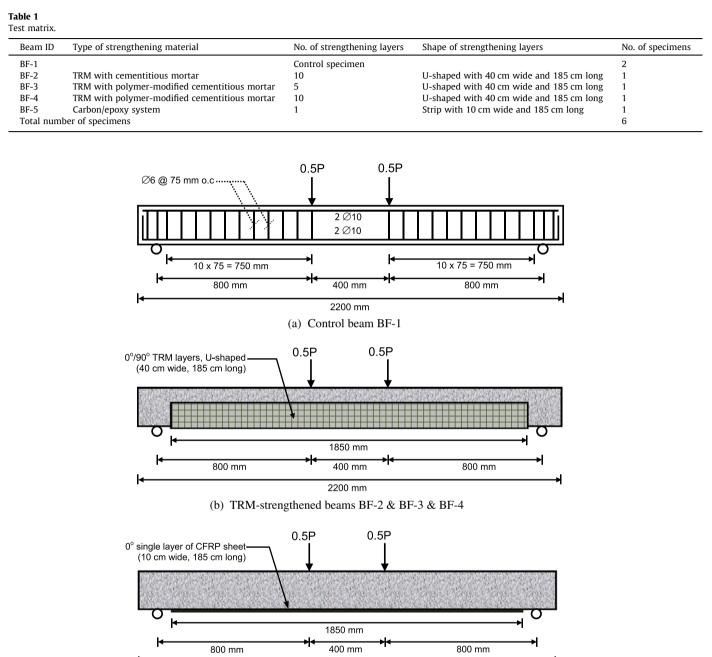
Bond conditions in cementitious composites could be improved and fiber–matrix interactions could be made tighter when continuous fiber sheets are replaced by textiles [2–5]. These materials comprise fabric meshes made of long woven, knitted or even unwoven fiber rovings in at least two (typically orthogonal) directions. The density, that is the quantity, and the spacing of rovings in each direction can be controlled independently, thus affecting the mechanical characteristics of the textile and the degree of penetration of the mortar matrix through the mesh. A literature review of studies on the use of textiles in the upgrading of concrete structures has revealed the following: the work reported in Curbach and Ortlepp [6] focused mainly on the bond between concrete and cement-based textile composites; the work in Curbach and Brueckner [7] presented test results on RC beams strengthened with two or three layers of alkaline resistant (AR) glass textile combined with cementitious mortar; and the work reported in Triantafillou et al. [2] demonstrated the effectiveness
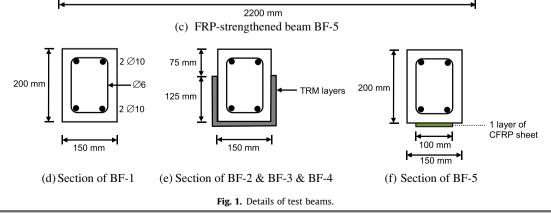
---

* Corresponding author. Tel.: +966 597938718.
  E-mail address: elsanadedy@yahoo.com (H.M. Elsanadedy).
[1] On leave from the Department of Civil Engineering, Helwan University, Cairo, Egypt.

of cement-based textile composites in the form of jackets to confine concrete in compression.

In a recent study, Larbi et al. [8] studied the mechanical feasibility of textile reinforced concrete plate for strengthening of RC beams by comparing them with traditional solutions such as carbon fiber-reinforced polymer (CFRP). Three distinct mortar-based composite mixes and two strengthening shapes were used, the U reinforcement and the side reinforcement, and compared with

Table 1
Test matrix.

Beam ID	Type of strengthening material	No. of strengthening layers	Shape of strengthening layers	No. of specimens
BF-1		Control specimen		2
BF-2	TRM with cementitious mortar	10	U-shaped with 40 cm wide and 185 cm long	1
BF-3	TRM with polymer-modified cementitious mortar	5	U-shaped with 40 cm wide and 185 cm long	1
BF-4	TRM with polymer-modified cementitious mortar	10	U-shaped with 40 cm wide and 185 cm long	1
BF-5	Carbon/epoxy system	1	Strip with 10 cm wide and 185 cm long	1
Total number of specimens				6

Fig. 1. Details of test beams.

CFRP results. The experimental study comprised of testing beams under three-point bending tests and measuring displacement at the mid-span and the strains in the transverse bars near the support. It was concluded based on the results from the study that, quantitatively the CFRP and the textile reinforced mortar materials have similar behavior, especially in the final stage. The results of the study indicated that a significant increase in the carrying capacity and bending stiffness was obtained by the use of mortar-based composite material. The U-shaped reinforced beams were found to be effective for the three distinct mortar-based composite mixes.

Test results from a study by Bruckner et al. [9] indicated that thin layers of concrete utilizing textile reinforcement can be used as shear strengthening for reinforced concrete T-beams thereby increasing the shear capacity of these beams. The shear strengthening provided by textile reinforced cement (TRC) was tested on T-beams designed deficient in shear. An anchoring system was also designed in order to sufficiently evaluate the bond anchoring outside of the compression zone. Based on the test results, it was concluded that the shear load carrying capacity of T-beams can be noticeably increased by applying TRC strengthening layers. However, the increase is only limited without the use of any mechanical anchoring of the strengthening layer.

Papanicolaou et al. [5] studied the effectiveness of using TRM composites in enhancing the flexural capacity of two-way RC slabs supported on edge beams. The TRM composites used comprised of carbon (or glass) fiber textiles externally bonded on the tension face of the slabs through the use of polymer-modified cement-based mortars. The experimental program involved testing four 2×2 m slab specimens supported on hinges at the corners. One slab was used as control specimen. One specimen received one layer of carbon fiber textile; another one received two, whereas the third specimen was strengthened with three layers of glass fiber textile having the same axial rigidity (in both directions) with the single-layered carbon fiber textile. All specimens failed due to flexural punching. The load-carrying capacity of the strengthened slabs was increased by 26%, 53% and 20% over that of the control specimen for slabs with one (carbon), two (carbon) and three (glass) textile layers, respectively. The strengthened slabs showed an increase in stiffness and energy absorption.

Recently, Al-Salloum et al. [10] investigated experimentally and numerically the effectiveness of TRM as a means of increasing the shear resistance of RC beams. Basalt-based textile was used as strengthening material. The studied parameters included type of mortar, number of textile layers and the orientation of the textile material. The experimental program comprised of testing 2 control beams, which were intentionally designed to be deficient in shear; in addition to testing 8 beams which were externally upgraded by TRM sheets for enhancing their shear capacity. It was concluded
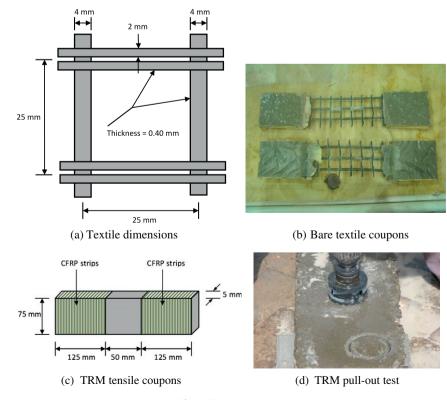
Table 2
Mechanical properties of TRM used in this study.

Mortar	
28-day tensile strength (MPa)	• 2.77 (cementitious mortar)
	• 3.4 (polymer-modified cementitious mortar)
28-day compressive strength (MPa)	• 23.9 (cementitious mortar)
	• 56.4 (polymer-modified cementitious mortar)
Bare basalt textile	
Tensile strength (MPa)	623
Elastic modulus (GPa)	31.94
Nominal thickness per layer[a] (mm)	0.064
TRM composite	
Tensile strength (MPa)	• 7.7 (cementitious mortar)
	• 8.23 (polymer-modified cementitious mortar)
Ultimate tensile strain	• 0.0299 (cementitious mortar)
	• 0.0536 (polymer-modified cementitious mortar)
Bond strength (MPa)	• 0.39 (cementitious mortar)
	• 0.70 (polymer-modified cementitious mortar)

[a] Based on equivalent smeared distribution of bare textile fibers.

(a) Textile dimensions

(b) Bare textile coupons

(c) TRM tensile coupons

(d) TRM pull-out test

Fig. 2. TRM test coupons.

that textile-mortar composite provides substantial gain in shear resistance; this gain is higher as the number of layers increases. With higher number of layers, textile with 45° orientation along with polymer-modified cementitious mortar provides the highest shear strength enhancement. Nonlinear finite element analysis was also carried out on the tested beams using LS-DYNA software [11]. Good agreement was achieved between the experimental and numerical results. The study was extended numerically to include additional cases with more TRM layers.

The present study is a continuation of the work carried out by Al-Salloum et al. [10], described briefly in the last paragraph. TRM composites comprising of basalt fiber textile along with two different mortar types were used for external flexural strengthening of RC beams. A total of six beams were tested under four-point bending till failure. The studied parameters included type of mortar (cementitious versus polymer-modified cementitious mortar), number of TRM layers as well as type of strengthening material (TRM versus CFRP composites). In addition to the experimental program, a numerical investigation utilizing nonlinear finite element analysis was carried out and a comparison was made between the experimental and numerical results. Based on the validation of results, the numerical study was extended to include additional cases to study the flexural enhancement of beams using more TRM layers with different end anchorages.

2. Experimental program

2.1. Test matrix

This study comprises of testing 6 simply supported small-scale RC beams ($150 \times 200 \times 2000$ mm) under 4-point loading. The criterion for selection of the beam dimensions was based on available resources in the laboratory. The beams were reinforced with $2\varnothing10$ longitudinal rebars on each side (top and bottom), at a cover of 25 mm. The shear reinforcement comprised of $\varnothing6$ stirrups at a small spacing of 75 mm, to ensure that failure would be controlled by flexural yielding. The goal is to study the effectiveness of TRM in enhancing the flexural capacity of RC beams. The test matrix is shown in Table 1. Two beams (BF-1(1) and BF-1(2)) were used as control specimens, which were intentionally designed to be under-reinforced with low reinforcement ratio so as to reveal the effectiveness of TRM composites in enhancing the flexural capacity. Three beams (BF-2, BF-3 and BF-4) were externally upgraded by TRM sheets. The last specimen (BF-5) was strengthened with single layer of CFRP laminates and it was designed to have the same flexural capacity as TRM-strengthened beam BF-3. Details of test beams are displayed in Fig. 1.

2.2. Properties of materials

2.2.1. Concrete and steel reinforcement

Ready-mix concrete with a specified compressive strength of 20 MPa was used to cast the beam specimens. For steel reinforcement, the average measured values for yield and tensile strengths of the 6 and 10 mm rebars were 280, 372 and 578, 684 MPa, respectively. After the curing period for the concrete beams, the specimens, which were to be strengthened, were thoroughly sand-blasted to remove dirt and any loose material. This was done to ensure optimum bond quality in between the concrete substrate and the TRM (or CFRP) layers. Markings were made on the specimens to outline the TRM (or CFRP) edges.

2.2.2. Textile reinforced mortar (TRM)

Two commercially available repair mortars (cementitious and polymer-modified cementitious) were utilized in this study. In or-

der to determine the compressive strength of mortar, 50-mm cubes were prepared and then tested in accordance with ASTM C109/C109M [12]. For measuring the tensile strength of mortar, briquette specimens were prepared for each mortar type and tested in accordance with ASTM C190 [13]. The measured properties of the two types of mortar used in this research are given in Table 2.

Basalt-based textile, with dimensions as shown in Fig. 2a, was used in this study. To obtain the mechanical properties of the textile used, five non-standard coupons of the bare textile were prepared and then tested in uniaxial tension (see Fig. 2b). Table 2 presents the measured mechanical properties of the bare textile.

In addition to tests on mortar and bare textile, tests were carried out on TRM coupons in order to measure tensile properties as well as bond strength between the TRM and the concrete substrate. Non-standard TRM tensile coupons were prepared for each mortar type using one layer of the basalt textile; at least five specimens were prepared of the dimensions given in Fig. 2c and then

Table 3
Material properties used in the finite element modeling of beams tested in this study.

Concrete	
Material model	MAT_CSCM_CONCRETE
Density (kg/m^3)	2320
Uni-axial compressive strength (MPa)	20
Max aggregate size (mm)	10
Mortar	
Material model	MAT_CSCM_CONCRETE
Density (kg/m^3)	1960
Uni-axial compressive strength (MPa)	• 23.9 (cementitious mortar) • 56.4 (polymer-modified cementitious mortar)
Max aggregate size (mm)	5
Longitudinal reinforcement	
Material model	MAT_PIECEWISE_LINEAR_PLASTICITY
Density (kg/m^3)	7850
Modulus of elasticity (MPa)	200,000
Poisson's ratio	0.30
Yield stress (MPa)	578
Plastic strain to failure	0.07658
Transverse reinforcement	
Material model	MAT_PIECEWISE_LINEAR_PLASTICITY
Density (kg/m^3)	7850
Modulus of elasticity (MPa)	200,000
Poisson's ratio	0.30
Yield stress (MPa)	280
Failure strain	0.19814
Basalt-based textile	
Material model	MAT_ENHANCED_COMPOSITE_DAMAGE
Density (kg/m^3)	1740
Young's modulus in the long. dir. (MPa)	31,940
Young's modulus in the transverse dir. (MPa)	31,940
Poisson's ratio	0.22
Shear modulus (MPa)	13,090
Longitudinal tensile strength (MPa)	623
Transverse tensile strength (MPa)	623
Carbon fiber reinforced polymer (CFRP) sheet[a]	
Material model	MAT_ENHANCED_COMPOSITE_DAMAGE
Thickness of each layer (mm)	1.0
Young's modulus in long. dir. (MPa)	77,300
Young's modulus in transverse dir. (MPa)	3380
Longitudinal tensile strength (MPa)	846
Transverse tensile strength (MPa)	40.6

[a] Results obtained from testing standard composite coupons in the lab.

tested under uniaxial tension till failure. In addition, standard pull-out tests in accordance with ASTM D4541 [14] as shown in Fig. 2d were carried out on TRM specimens, adhered to an existing concrete substrate. Results of tension and pull-out tests are summarized in Table 2.

For TRM-upgraded specimens, a layer of mortar about 2 mm thick was applied on the beam specimens first using a metal trowel. The textile was then pressed slightly into the mortar until the mortar protruded out of the perforations between the rovings. The second mortar layer was then applied to completely cover the
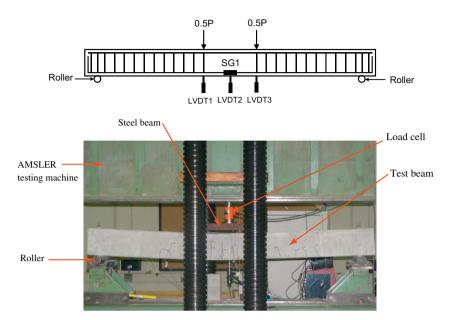

Fig. 3. Test setup and instrumentation.

Table 4
Load and mode of failure comparison for all beams.

Beam ID	Axial stiffness per unit length of strengthening layers[a] (kN/mm)	Axial capacity of strengthening layers[b] (kN)	Yield load (P_y) (kN)			Ultimate load (P_u) (kN)			Mode of failure	
			EXP	FEM	EXP/FEM	EXP	FEM	EXP/FEM	EXP	FEM
Beams tested in this study										
BF-1(1)	0	0	37.18	35.92	1.04	43.22	39.70	1.09	CC	CC
BF-1(2)	0	0	34.39	35.92	0.96	42.28	39.70	1.06	CC	CC
BF-2	8177	155	45.89	47.65	0.96	77.63	77.97	1.00	End DB	End DB
BF-3	4088	78	40.12	42.43	0.95	59.46	61.97	0.96	FR	FR
BF-4	8177	155	46.98	50.72	0.93	81.75	84.59	0.97	FR	FR
BF-5	7730	77	44.89	46.99	0.96	64.10	65.89	0.97	FR	FR
Beams tested by Papanicolaou et al. [4]										
C_fl	0	0	NA	73.95	–	83.50	79.09	1.06	CC	CC
M4_fl	5076	76	NA	84.99	–	111.00	112.07	0.99	End DB	End DB
R4_fl	5076	76	NA	84.97	–	125.00	120.24	1.04	FR	FR

CC: concrete crushing; FR: textile (or FRP) rupture; end DB: TRM (or FRP) end debonding.
[a] Axial stiffness per unit length of strengthening layers = Young's modulus × reinforcement area.
[b] Axial capacity of strengthening layers = Young's modulus × reinforcement area × rupture strain of the textile (or CFRP) reinforcement.

Table 5
Mid-span deflection and ductility comparison for all beams.

Beam ID	Mid-span deflection at yield load (Δ_y) (mm)			Mid-span deflection at ultimate load (Δ_u) (mm)			Deflection ductility ratio ($\mu_\Delta = \Delta_u/\Delta_y$)		
	EXP	FEM	EXP/FEM	EXP	FEM	EXP/FEM	EXP	FEM	EXP/FEM
Beams tested in this study									
BF-1(1)	8.87	9.69	0.92	86.19	84.90	1.02	9.72	8.76	1.11
BF-1(2)	8.85	9.69	0.91	81.74	84.90	0.96	9.24	8.76	1.05
BF-2	9.95	10.00	0.99	40.28	41.50	0.97	4.05	4.15	0.98
BF-3	9.09	9.47	0.96	34.15	36.33	0.94	3.76	3.84	0.98
BF-4	9.18	10.00	0.92	42.44	44.93	0.94	4.63	4.49	1.03
BF-5	9.42	10.25	0.92	22.05	25.75	0.86	2.34	2.51	0.93
Beams tested by Papanicolaou et al. [4]									
C_fl	NA	8.10	–	42.00	43.98	0.96	–	5.43	–
M4_fl	NA	8.14	–	24.00	24.53	0.98	–	3.01	–
R4_fl	NA	7.60	–	22.20	25.40	0.87	–	3.34	–

textile fabric and the procedure was repeated for each layer of TRM. Each layer was applied prior to the previous layer becoming dry.

2.2.3. CFRP system

In the present study, Carbon FRP sheets supplied by Fyfe Company were employed for the strengthening of specimen BF-5. The coupon samples were cut from the sheets to determine the average mechanical properties of the sheets. The average coupon test results of CFRP system are shown in Table 3. On the clean and flat bottom surface of beam BF-5, primer, epoxy, and single layer of CFRP laminates were applied in sequence.

2.3. Test setup

The six beams were subjected to 4-point bending at a total span of 2.0 m and a shear span of 0.8 m. The load was applied using a stiff steel beam connected to 2000-kN AMSLER testing machine. A load cell was mounted between the machine and the rigid beam as shown in Fig. 3 in order to record load during the experiment. All specimens were monotonically loaded at a displacement rate of 1 mm/min till failure. Three LVDTs were affixed underneath the beams to measure their deflections during the test. Moreover, strain gages were used to record strains at the level of steel reinforcement during the experiment. The sensor locations are shown in Fig. 3.

3. Test results and discussion

Tables 4 and 5 show a summary of the flexural behavior of all test beams in terms of flexural loading capacity, failure mode, mid-span deflection and ductility. In order to get an estimation of the efficiency of the strengthening systems used and to help in the comparison of the results, both axial stiffness and axial capacity of the TRM (or CFRP) layers were calculated for all strengthened beams as shown in Table 4. Load versus mid-span deflection curves are presented as shown in Fig. 4 for all test beams. In addition, final modes of failure are illustrated in Fig. 5 for representative samples of test beams. As demonstrated in Fig. 4, the two control specimens BF-1(1) and BF-1(2) displayed the standard nearly-bilinear response characteristics of under-reinforced beams. They failed in flexure through the formation of wide flexural crack at the mid-span with the final mode of failure being concrete crushing at the critical section as presented in Fig. 5a. The average ultimate load and deflection ductility of the two beams were 42.75 kN and 9.48, respectively.
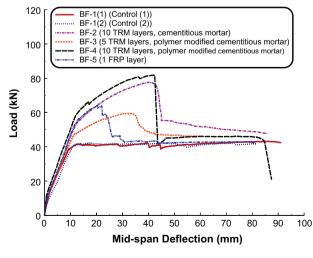

Fig. 4. Load–deflection curves for test beams.

For the two TRM-strengthened beams BF-2 and BF-4, having the same number of TRM layers with different mortar types, it was observed that at maximum load of 77.63 kN, specimen BF-2 failed suddenly due to TRM debonding at the right end as displayed in Fig. 5b. However, at maximum load of 81.75 kN, beam BF-4 failed due to textile rupture near the mid-span (see Fig. 5c). Upon failure, the flexural capacity of the two beams dropped down suddenly with the final mode of failure being due to concrete crushing at the end of the test (similar to what was observed for the two control specimens). The deflection ductility was estimated as 4.05 and 4.63, for beams BF-2 and BF-4, respectively. This brings about, the conclusion that polymer-modified cementitious mortar is better than cementitious mortar in terms of ensuring the full bond action between the TRM layers and the concrete substrate and hence increasing the flexural capacity and deflection ductility.

As mentioned previously, the two strengthened beams BF-3 and BF-5 were designed to have the same flexural capacity. This may be verified by comparing the axial capacity of the strengthening layers of the two beams as demonstrated in Table 4. Failure was due to textile and CFRP rupture (see Fig. 5d) near the mid-span of specimens BF-3 and BF-5, respectively. Upon textile (or CFRP) rupture, the flexural capacity dropped down (gradually for beam BF-3 and suddenly for specimen BF-5) to a value close to that of the two control specimens. The final mode of failure for the two specimens was similar to the control beams where concrete crushing was observed at the end of the test. The TRM-strengthened beam (BF-3) displayed similar characteristics to its FRP-strengthened counterpart (specimen BF-5), with three distinct differences: its response was more ductile (61% more effective in terms of deflection ductility); yielding initiated at a lower load and the ultimate load was slightly lower (7.2% less effective in terms of flexural strength).

4. Beams tested by Papanicolaou et al. [4]

In addition to the six beams tested in this study, three other specimens tested by Papanicolaou et al. [4] were used for calibrating the finite element modeling conducted in this study. Papanicolaou et al. [4] investigated the effectiveness of TRM as externally applied flexural strengthening reinforcement of RC beams. Three under-reinforced beams were tested in four-point bending, at a span length of 2.0 m and a shear span of 0.75 m. The beams had a cross section of 150×250 mm and were reinforced with $2\varnothing12$ longitudinal rebars on each side (top and bottom), at a cover equal to 25 mm. The shear reinforcement comprised of $\varnothing8$ stirrups at a spacing of 100 mm, to ensure that failure would be controlled by flexural yielding. Self-compacting concrete with mean 28-day compressive strength of 34.5 MPa was used for the casting of the beams. The steel reinforcement had an average yield stress equal to 530 MPa. One of the three beams was tested without strengthening, as a control specimen (C_fl); a second one was strengthened with four layers of carbon fiber textile bonded with cement-based mortar (M4_fl); the third beam was identical to the second one but with an epoxy resin-based matrix material for the textile reinforcement (R4_fl). The externally bonded reinforcement had a width and a length equal to 120 mm and 1.90 m, respectively, so that its distance from each support was equal to 50 mm. The carbon fiber textile used in specimens M4_fl and R4_fl had: a nominal thickness of each layer (corresponding to the equivalent smeared distribution of fibers) of 0.047 mm, a tensile strength of 3350 MPa and an elastic modulus of 225 GPa. The mortar used for specimen M4_fl had 28-day compressive and flexural strengths of 30.61 and 4.24 MPa, respectively. The experimental loads versus mid-span deflection for the three beams are given in Fig. 9a–c. The control specimen (C_fl) failed in flexure. The FRP-strengthened

Concrete crushing

(a) Control beam BF-1

TRM end debonding

(b) BF-2

(c) BF-4

Textile rupture
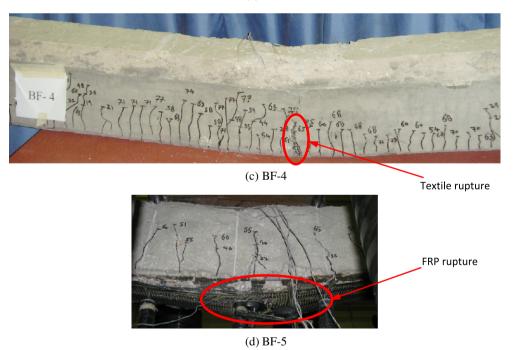
FRP rupture

(d) BF-5

Fig. 5. Mode of failure for representative samples of test beams.

beam (R4_fl) failed by the tensile fracture of the externally bonded reinforcement at mid-span (at a load of 125 kN). However, for the TRM-strengthened beam (M4_fl) the ultimate load was lower (111 kN); and the failure mechanism was governed by debonding at the end (anchorage) of the external reinforcement due to inter-laminar shearing. Summary of test results of the three beams is shown in Tables 4 and 5.

5. Finite element modeling

LS-DYNA [11], a general-purpose finite element program, was employed for the numerical simulation of the TRM-strengthened beams under four-point bending tests. The 3-D finite element model was developed using a general-purpose pre-processor

FEMB. Only half of the beam was modeled accounting for its symmetry.

5.1. Model geometry

In order to mimic the real behavior of tested RC beams, it is imperative that the concrete volume be modeled using solid elements. For this reason, 8-node reduced integration solid elements were used to model the concrete. The longitudinal reinforcing bars and the transverse ties were modeled using 2-node Hughes Lui beam elements. The basalt-based textile and the carbon/epoxy composite were modeled using 4-node shell elements. The Belytschko-Tsay [15] element formulation was used for all shell elements. For RC beams tested in this study, the basalt-based

textile, arranged in two orthogonal directions, was smeared into orthotropic material with an equivalent thickness of 0.064 mm per layer. Finally, 8-node solid elements were used to model the mortar.

The concrete volume was modeled by cube elements with maximum size of 25 mm. Numerical convergence study showed that further decrease in the mesh size has little effect on the numerical results but leads to the risk of computer memory overflow and substantially increases the computing time. Fig. 6 shows the typical mesh of the TRM-strengthened beam.

5.2. Material modeling

The material model type 159, MAT_CSCM_CONCRETE was employed to model both the concrete for the beam and the mortar for the TRM. This is a smooth or continuous cap model available in LS-DYNA for solid elements, with a smooth intersection between the shear yield surface and the hardening cap. In this model, the initial damage surface coincides with the yield surface. Rate effects are modeled with viscoplasticity. More details of this material model can be found in references [16,17].

For modeling the steel reinforcement, material model type 24, MAT_PIECEWISE_LINEAR_PLASTICITY was used. This material is suited to model elasto-plastic materials with an arbitrary stress versus strain curve and an arbitrary strain rate dependency. In order to model the textile material and the CFRP sheets, the material model type MAT_054-055, MAT_ENHANCED_COMPOSITE_DAMAGE was employed. An orthotropic material with optional brittle failure can be defined using this material card. Various failure criteria are possible for this card. The failure criterion of Chang and Chang [18] was used in this study. The part composite card was used to input the textile and carbon fiber properties. This card allows the input of material ID, composite thickness and material orientation for each of the composite layers. A summary of the

material properties used for beams tested in this study is presented in Table 3.

5.3. Erosion

The erosion option provides a way of including failure to the material models. This is not a material or physics based property; however, it lends a great means to imitate concrete spalling phenomena and produce graphical plots which are more realistic representations of the actual events. By activating this feature, the eroded solid element is physically separated from the rest of the mesh. Material failure was simulated by element erosion at a specific plastic strain; thus, whenever an element reaches this critical value, it is removed from the computation. This erosion model represents a numerical remedy to distortion, which can cause excessive and unrealistic deformation of the mesh. In this study, elements of concrete and mortar were allowed to erode when the maximum principal strain reached 0.05 [17].

5.4. Contact modeling

Bond between TRM (or CFRP) layers and concrete substrate was modeled through the tiebreak surface-to-surface contact definition of LS-DYNA. Tiebreak contact is a special type of contact. It works the same as common contact types under compressive load. The contact algorithm accounts for both normal and shear forces in the interface. Under tensile and shear loads, tiebreak allows the separation of the tied surfaces following an interface strength-based failure criterion. The following failure criterion was used in this work:

$$\left(\frac{|\sigma_n|}{NFLS}\right)^2 + \left(\frac{|\sigma_s|}{SFLS}\right)^2 \geqslant 1 \tag{1}$$
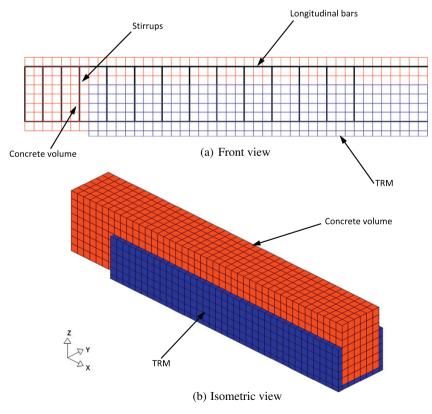

Fig. 6. Finite element mesh in FEMB software showing the modeled components.

where σ_n is the normal stress, σ_s is the shear stress, *NFLS* is the normal failure stress and *SFLS* is the shear failure stress. After failure, this contact type behaves as a surface-to-surface contact with no thickness offsets. In addition, after failure, no interface tension is possible. In the present study, the concrete substrate was considered as master surface whereas the TRM (or CFRP) layers were used as slave surface. The most difficult part in this contact modeling is the estimation of the failure stresses *NFLS* and *SFLS*. Improper values for *NFLS* and *SFLS* may lead to erroneous results. These failure stresses should be estimated from either pull-out testing of the two tied materials or validated through empirical models. The failure parameters used in the present work were estimated as follows:

5.4.1. TRM-strengthened beams

For the three TRM-strengthened beams tested in this study (BF-2, BF-3 and BF-4), the normal failure stress of the contact (*NFLS*) was input as the measured pull-out bond strength values listed in Table 2. For beams with polymer-modified cementitious mortar

(BF-3 and BF-4) and since TRM debonding was not observed in the experimental testing, the shear failure stress (*SFLS*) was taken as the minimum tensile strength of the two materials in contact (mortar and concrete substrate) based on the ACI 318-11 [19] as follows:

$$SFLS = 0.62\sqrt{\min(f_c^{/};f_m^{/})} \quad (\text{MPa}) \tag{2}$$

where $f_c^{/}$ = specified compressive strength of concrete substrate and $f_m^{/}$ = compressive strength of TRM mortar. Yet, for beam BF-2 with cementitious mortar in which TRM end debonding was noticed in the test, the shear failure stress (*SFLS*) was reduced in proportion with its lower pull-out bond strength. For beam BF-2, the shear failure stress was taken as 56% of that given by Eq. (2). For the TRM-strengthened specimen tested by Papanicolaou et al. [4] (M4_fl), no measured values were available for *NFLS* & *SFLS*. Therefore, the shear failure stress (*SFLS*) was estimated from Eq. (2); however, the normal failure stress (*NFLS*) was calculated based on the work of Silfwerbrand [20] from:
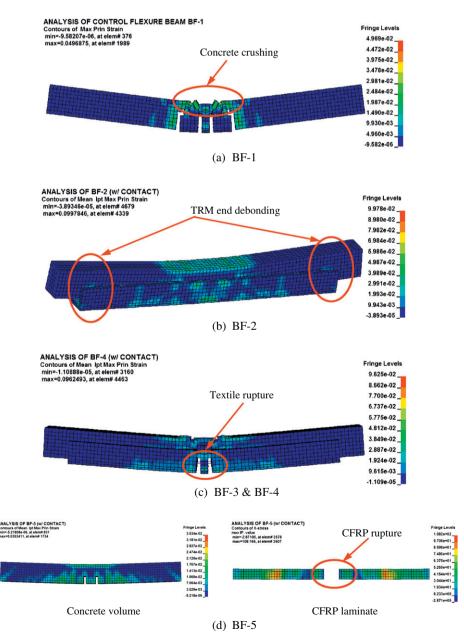

(a) BF-1

(b) BF-2

(c) BF-3 & BF-4

Concrete volume   CFRP laminate

(d) BF-5

Fig. 7. FE mode of failure for beams tested in this study.

$$NFLS = \frac{SFLS}{3.1} \qquad (3)$$
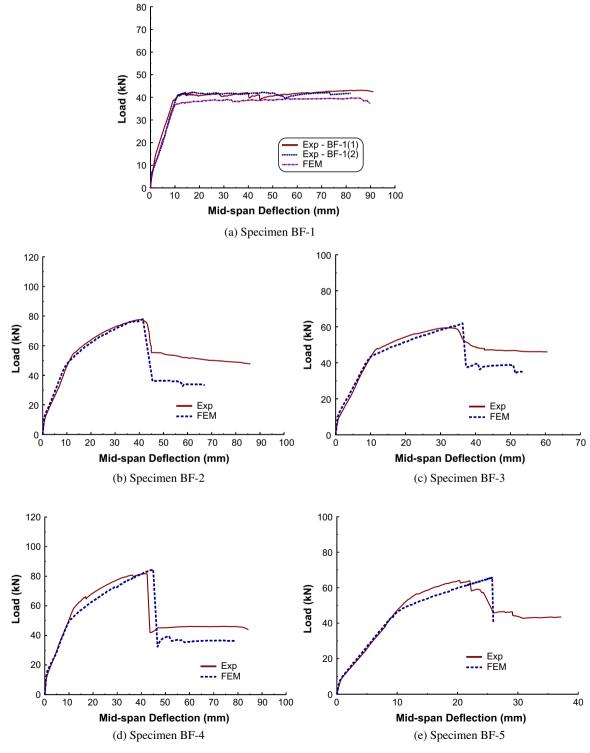
$$SFLS = 1.5\beta_w NFLS \qquad (5)$$

where

5.4.2. FRP-strengthened beams

For FRP-to-concrete contact, the failure parameters were estimated based on Neale et al. [21] as follows:

$$\beta_w = \sqrt{\frac{2.25 - b_f/b_c}{1.25 + b_f/b_c}} \qquad (6)$$

$$NFLS = 0.62\sqrt{f_c'} \quad \text{(MPa)} \qquad (4)$$

where b_f = width of FRP laminates and b_c = width of RC beam.

(a) Specimen BF-1

(b) Specimen BF-2

(c) Specimen BF-3

(d) Specimen BF-4

(e) Specimen BF-5

Fig. 8. Load–deflection comparison for beams tested in this study.

5.5. Boundary conditions

Only half of the beam was modeled in LS-DYNA taking into account the symmetry of the beam specimens. A node set was cre-ated which consisted of nodes at support location of the beam which had to be restricted for the displacement in the global *Z* direction. This translates as a roller support near the beam end.

(a) Specimen C_fl

(b) Specimen M4_fl

(c) Specimen R4_fl
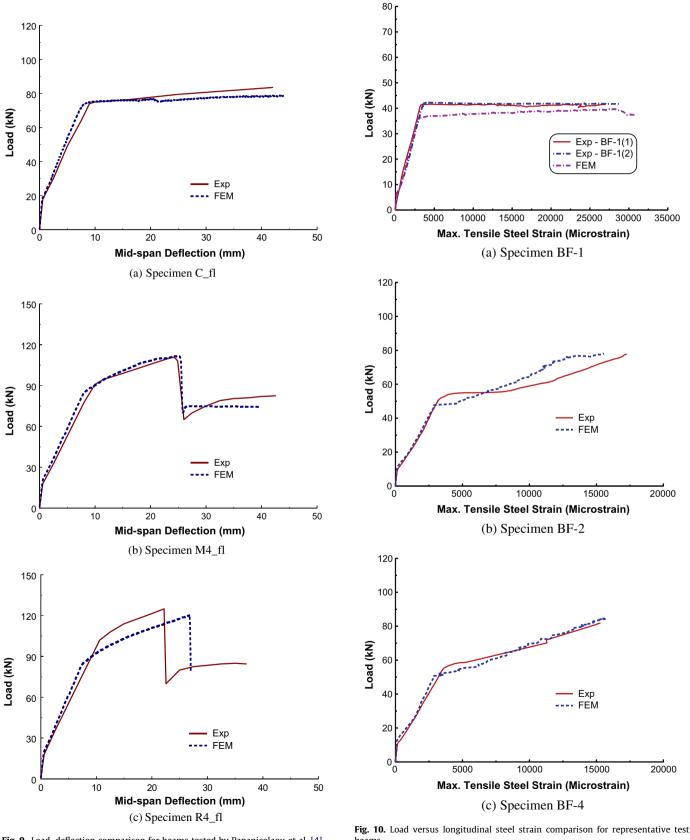
Fig. 9. Load–deflection comparison for beams tested by Papanicolaou et al. [4].

(a) Specimen BF-1

(b) Specimen BF-2

(c) Specimen BF-4

Fig. 10. Load versus longitudinal steel strain comparison for representative test beams.

Table 6
Steel and TRM (or FRP) strain comparison for beams tested in this study.

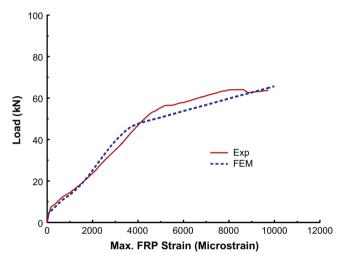| Beam ID	Tensile steel strain at ultimate load ($\mu\varepsilon$)			TRM (or FRP) strain at ultimate load ($\mu\varepsilon$)		
	EXP	FEM	EXP/FEM	EXP	FEM	EXP/FEM
BF-1(1)	27,058	28,149	0.96	–	–	–
BF-1(2)	28,669	28,149	1.02	–	–	–
BF-2	17,236	15,550	1.11	NA	17,326	–
BF-3	NA	14,137	–	NA	19,343	–
BF-4	15,272	15,457	0.99	NA	19,430	–
BF-5	NA	11,002	–	9712	9993	0.97

Fig. 11. Load versus FRP strain comparison for beam BF-5.

Symmetric boundary conditions were applied for the nodes in elements for the plane representing the continuation of the beam in reality. This included restriction of displacement in the global X direction and the rotation about the global Y and Z directions for those nodes. Since the loading was displacement controlled, another node set was created which comprised of nodes along the loading plane which were controlled to have the same Z-displacement throughout the test.

5.6. Loading strategy

LS-DYNA uses explicit time integration algorithms for solving the problems, which are less sensitive to machine precision than other finite element solution methods. The load application process in LS-DYNA is time-history dependent. Since the testing procedure involved displacement controlled static loading, the inertia effects were removed from the dynamic equation by assigning a constant velocity to the displacement controlled node set. This will lead to zero acceleration and hence zero inertia force. The rate of change of displacement was defined as 1 mm/min to match with the experimental loading.

Table 7
Details of TRM-strengthened specimens used in the finite element analysis.

Beam ID	Beam dimensions (mm)				f_c' (MPa)	Longitudinal steel		TRM properties			f_m' (MPa)	E_f (GPa)	f_{fu} (MPa)
	b	h	L	a		No. and diameter	f_y (MPa)	n	t_f (mm)	Shape of strengthening layers			
BF-2	150	200	2000	800	20	2∅10	578	10	0.064	U-shaped with 40 cm wide and 185 cm long	23.9	31.94	623
BF-3	150	200	2000	800	20	2∅10	578	5	0.064	U-shaped with 40 cm wide and 185 cm long	56.4	31.94	623
BF-4	150	200	2000	800	20	2∅10	578	10	0.064	U-shaped with 40 cm wide and 185 cm long	56.4	31.94	623
BF-6	150	200	2000	800	20	2∅10	578	12	0.064	U-shaped with 40 cm wide and 185 cm long	56.4	31.94	623
BF-7	150	200	2000	800	20	2∅10	578	15	0.064	U-shaped with 40 cm wide and 185 cm long	56.4	31.94	623
BF-8	150	200	2000	800	20	2∅10	578	20	0.064	U-shaped with 40 cm wide and 185 cm long	56.4	31.94	623
M2_fl	150	250	2000	750	34.5	2∅12	530	2	0.047	Strip with 12 cm wide and 190 cm long – without end anchorage	30.61	225	3350
M2_fl_U	150	250	2000	750	34.5	2∅12	530	2	0.047	Strip with 12 cm wide and 190 cm long – with end anchorage	30.61	225	3350
M4_fl	150	250	2000	750	34.5	2∅12	530	4	0.047	Strip with 12 cm wide and 190 cm long – without end anchorage	30.61	225	3350
M4_fl_U	150	250	2000	750	34.5	2∅12	530	4	0.047	Strip with 12 cm wide and 190 cm long – with end U-anchorage	30.61	225	3350
M6_fl	150	250	2000	750	34.5	2∅12	530	6	0.047	Strip with 12 cm wide and 190 cm long – without end anchorage	30.61	225	3350
M6_fl_U	150	250	2000	750	34.5	2∅12	530	6	0.047	Strip with 12 cm wide and 190 cm long – with end U-anchorage	30.61	225	3350
M8_fl	150	250	2000	750	34.5	2∅12	530	8	0.047	Strip with 12 cm wide and 190 cm long – without end anchorage	30.61	225	3350
M8_fl_U	150	250	2000	750	34.5	2∅12	530	8	0.047	Strip with 12 cm wide and 190 cm long – with end U-anchorage	30.61	225	3350
M10_fl	150	250	2000	750	34.5	2∅12	530	10	0.047	Strip with 12 cm wide and 190 cm long – without end anchorage	30.61	225	3350
M10_fl_U	150	250	2000	750	34.5	2∅12	530	10	0.047	Strip with 12 cm wide and 190 cm long – with end U-anchorage	30.61	225	3350
M12_fl	150	250	2000	750	34.5	2∅12	530	12	0.047	Strip with 12 cm wide and 190 cm long – without end anchorage	30.61	225	3350
M12_fl_U	150	250	2000	750	34.5	2∅12	530	12	0.047	Strip with 12 cm wide and 190 cm long – with end U-anchorage	30.61	225	3350

b = Width of beam section.
h = Depth of beam section.
L = Beam span.
a = Beam shear span.
f_y = Yield strength of longitudinal steel.
n = Number of plies of TRM reinforcement.
t_f = Nominal thickness of one ply of the textile reinforcement.
f_m' = Compressive strength of mortar.
E_f = Tensile modulus of elasticity of textile reinforcement.
f_{fu} = Tensile strength of textile reinforcement.

6. Finite element results and discussion

6.1. Modes of failure

Fig. 7 depicts the modes of failure for beams tested in this study as observed from the FE analysis post-processing software. The failure modes are based on contours of mid-surface maximum principal strains. It is noted that the failure modes predicted from the FE analysis matches very well with the experimental observations. From the analysis it was found that, the control beam BF-1 failed due to concrete crushing after the formation of wide flexural cracks in the maximum moment region as depicted in Fig. 7a. As presented in Fig. 7b, specimen BF-2 failed due to TRM end debonding after reaching a maximum textile stress of 553 MPa. However, as seen in Fig. 7c, beams BF-3 and BF-4 failed by textile rupture at midspan after the textile attained its maximum stress. Fig. 7d incorporates the failure mode, as per the analysis, for the CFRP-strengthened specimen BF-5 which failed in flexure due to FRP rupture in the maximum moment region.

6.2. Load–deflection curves

A comparison was made between the load–deflection curves obtained from the experimental and the numerical studies for all beam specimens tested in this study and by Papanicolaou et al. [4]. Figs. 8 and 9 depict this comparison. As seen from the figures, the experimental load–deflection curves showed good agreement especially for the ultimate load carrying capacity, compared with the FE analysis of the control beams as well as TRM- and FRP-strengthened beams. For all TRM-strengthened beams, the ultimate load carrying capacity and the mid-span deflection in the plastic region were only slightly higher for the numerical results. Tables 4 and 5 enlist the comparison details. As seen in Table 4, maximum deviations of 7% and 9% were found for the numerical results for yield and ultimate loads, respectively. Yet, compared with the experimental results, maximum deviations of 9%, 14% and 11% were observed for mid-span deflection at yield load, mid-span deflection at ultimate load and deflection ductility, respectively. The stiffness of the beam specimens was also
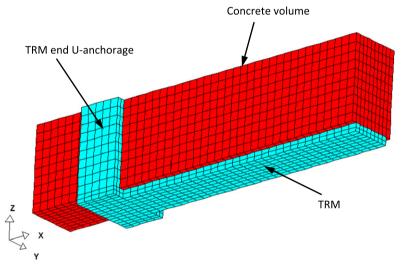

Fig. 12. Finite element mesh showing end U-anchorage for specimen M12_fl_U.

Table 8
FE analysis results for TRM-strengthened beams.

Beam ID	Yield load (P_y) (kN)	Ultimate load (P_u) (kN)	Mid-span deflection at yield load (Δ_y) (mm)	Mid-span deflection at ultimate load (Δ_u) (mm)	Deflection ductility ratio ($\mu_\Delta = \Delta_u/\Delta_y$)	Textile stress at ultimate load (MPa)	Mode of failure
Group 1: Beams of this study							
BF-3	42.43	61.97	9.47	36.33	3.8	618	FR
BF-4	50.72	84.59	10.00	44.93	4.5	621	FR
BF-6	53.18	90.08	10.15	44.73	4.4	619	FR
BF-7	58.71	96.11	11.15	40.82	3.7	505	End DB
BF-8	65.85	93.62	11.11	27.91	2.5	327	End DB
Group 2: Beams of Papanicolaou et al. [4] (with end U-anchorage)							
M2_fl_U	79.47	99.29	7.97	24.27	3.0	3324	FR
M4_fl_U	85.66	121.09	8.05	29.66	3.7	3342	FR
M6_fl_U	91.02	142.67	8.19	31.70	3.9	3347	FR
M8_fl_U	97.92	149.04	8.41	26.12	3.1	2751	End DB
M10_fl_U	102.65	157.60	8.42	23.73	2.8	2431	End DB
M12_fl_U	108.81	160.85	8.55	20.80	2.4	2080	End DB
Group 3: Beams of Papanicolaou et al. [4] (without end U-anchorage)							
M2_fl	79.47	99.29	7.97	24.27	3.0	3324	FR
M4_fl	84.99	112.07	8.14	24.53	3.0	2644	End DB
M6_fl	91.71	117.70	8.48	18.13	2.1	2035	End DB
M8_fl	98.49	120.61	8.76	16.30	1.9	1616	End DB
M10_fl	102.46	115.47	8.64	11.82	1.4	1170	End DB
M12_fl	109.77	117.36	9.01	10.61	1.2	1014	End DB

FR: textile rupture; END DB: TRM end debonding.

predicted efficiently by the FE models in comparison with the experimental results. Figs. 8 and 9 also show that the FE models were successful in imitating the softening behavior which demonstrates the accuracy of the material model.

Comparing the numerical results of beams BF-2 and BF-4, it is clear that the FE analysis supported the conclusion that polymer-modified cementitious mortar is better than cementitious mortar in terms of enhancing the beam's flexural capacity and deflection ductility. In addition, the FE results evidenced that TRM-strengthened beams BF-3 and M4_fl had slightly lower flexural capacity with more ductility response compared with their FRP counterparts BF-5 and R4_fl, respectively.

6.3. Strain gage results

The maximum tensile strain in the longitudinal steel obtained from the post-processing software of LS-DYNA for the tested beam specimens was compared with the experimental steel strains obtained using the strain gages. Fig. 10a–c depicts this comparison for beams BF-1, BF-2 and BF-4, respectively. For all other beams, experimental steel strains were not available. Table 6 enlists measured and predicted steel strains for beam specimens tested in this study. Good agreement was achieved between the experimental and predicted steel strains. It is clear that the two control specimens BF-1(1) and BF-1(2) had a high ductile behavior with an average strain ductility (ratio of steel strain at ultimate load to steel yield strain) of 9.6, which is typical for such under-reinforced beams failing in flexure. Nevertheless, a strain ductility of more than 4.9 was obtained for TRM-strengthened beams BF-2, BF-3 and BF-4, which is significantly more than the corresponding value of 3.8 for FRP-strengthened beam BF-5. In addition to longitudinal steel, strain gages were attached to TRM (or FRP) laminates to record their strain throughout the test. Unfortunately, due to mortar cracking, strain gages affixed to the TRM were damaged at early stages during the testing of beams BF-2 to BF-4; yet, FRP strain was successfully recorded up to the maximum load level of beam BF-5. Fig. 11 shows the FRP strain comparison for BF-5 where good agreement was attained between the experimental and predicted curves.

7. Effect of number of layers and end condition of TRM composites

The FE analysis was utilized to study the effect of number of layers and end condition of TRM laminates on the flexural performance of strengthened beams. In addition to the four TRM-strengthened beams used for FE validation (BF-2 to BF-4 and M4_fl), another fourteen specimens were numerically investigated. Details of all beams used in the finite element analysis are listed in Table 7. It should be noted that the three specimens BF-6 to BF-8 have the same dimensions and material properties as those used for BF-3 and BF-4, yet, with 12, 15 and 20 layers, respectively. Specimens M2_fl, M6_fl, M8_fl, M10_fl and M12_fl have the same dimensions and material properties as beam M4_fl, but with 2, 6, 8, 10 and 12 TRM layers, respectively. Beams M2_fl_U, M4_fl_U, M6_fl_U, M8_fl_U, M10_fl_U and M12_fl_U are the same as their counterparts M2_fl to M12_fl except with the addition of TRM end U-anchorage as displayed from the FE mesh shown in Fig. 12.

In order to study the effect of number of TRM layers and end condition on the flexural behavior of TRM-strengthened beams, a new bond related parameter called "bond-stiffness coefficient (α_b)" was first introduced in this study. This coefficient is the ratio of TRM stiffness to its tensile bond strength, as given from the following formula:
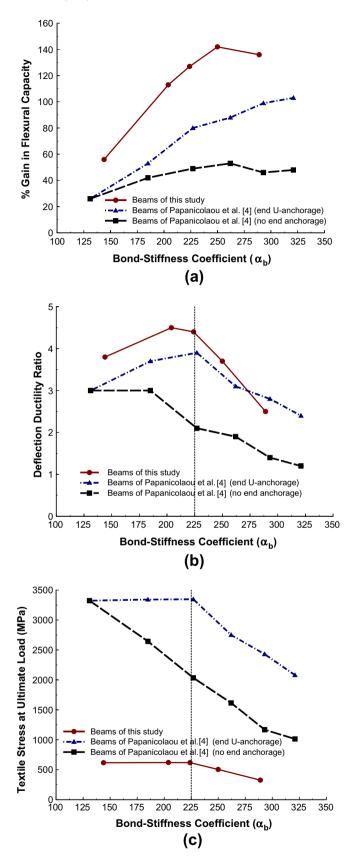
$$\alpha_b = \frac{\sqrt{nE_f t_f}}{NFLS} \tag{7}$$

(a)

(b)

(c)

Fig. 13. Relationship between bond-stiffness coefficient (α_b) and response parameters for TRM-strengthened beams (based on FE analysis).

where n = number of TRM layers, E_f = tensile modulus of textile reinforcement (in MPa) and t_f = equivalent smeared thickness of single layer of textile reinforcement (in mm) and $NFLS$ = tensile

bond strength between TRM and concrete substrate (in MPa). It is worth mentioning that the numerator in the right hand side of the above equation is a measure of the TRM stiffness and is based on formula (10-2) of the ACI 440.2R-08 [22] used for the estimation of FRP debonding strain in FRP-strengthened beams.

Summary of FE analysis results for TRM-strengthened beams is listed in Table 8. It should be noted that in Table 8, the TRM-strengthened beams are divided into three groups, *viz.* group (1) is for beams of this study; group (2) is for beams of Papanicolaou et al. [4] with end U-anchorage and group (3) is for beams of Papanicolaou et al. [4] without end U-anchorage. It is clear that for beams of group (1), TRM rupture was observed for beams with 5, 10 and 12 layers for which the gain in the flexural capacity (with respect to control specimen BF-1) was 56%, 113% and 127%, respectively. For beams BF-7 and BF-8 with 15 and 20 layers, respectively, the ultimate loads were close to the shear capacity and end debonding was predicted due to diagonal shear crack at the end of the TRM layers. For group (2), it is noticed that TRM rupture was predicted for beams with 2, 4 and 6 layers, for which the flexural capacity gain was 26%, 53% and 80%, respectively. However, TRM end debonding was evident for beams with 8, 10 and 12 layers. For group (3), TRM rupture was only predicted for beam M2_fl with 2 layers and all other beams failed due to debonding at the end of TRM layers. Comparing the results of groups (2) and (3), it is clear that the end U-anchorage was effective in beams with more than 2 layers. The end U-anchorage increased the flexural capacity for beams M4_fl_U, M6_fl_U, M8_fl_U, M10_fl_U and M12_fl_U by 8%, 21%, 24%, 36% and 37% over their corresponding beams without end anchorage. It can be generally concluded that the provision of end U-anchorage was efficient in preclusion or even delaying the TRM end debonding.

The relationship between the bond-stiffness coefficient (α_b) and the response parameters is shown in Fig. 13a–c for percent gain in flexural capacity, deflection ductility ratio and textile stress at ultimate load level, respectively. It is evident that for beams of groups (1) and (2) in which TRM layers are well anchored at the end, the TRM composites were effective in enhancing the flexural capacity up to bond-stiffness coefficient of 225, after which both ultimate textile stress and deflection ductility were significantly reduced due to TRM end debonding. For beams of group (1), when the bond-stiffness coefficient reached a value of 250, the flexural capacity was very close to the beam's shear capacity and the gain in the flexural capacity decreased from 142% to 136% when the bond-stiffness coefficient increased from 250 to 290. However, for beams of group (2), the gain in flexural capacity increased from 80% to 99% as the bond-stiffness coefficient increased from 225 to 290, after which insignificant increase in flexural capacity was achieved. At a bond-stiffness coefficient of 290, debonding occurred at a textile stress level of about 73% of its tensile strength.

8. Conclusions

The major conclusions derived from this study are as follows:

1. Based on the experimental testing conducted in this study, it is indicated that polymer-modified cementitious mortar provided better bond between TRM layers and concrete substrate than cementitious mortar. The basalt textile-reinforced mortar layers added substantial gain in the flexural capacity of RC beams ranging from 39% to 91%.
2. From the results obtained in this study it was shown that compared with its FRP counterpart, TRM-based strengthening system is slightly less effective in terms of enhancing the flexural strength of RC beams but more effective in terms of deflection ductility.

3. Based on the FE analysis carried out in this study, it can be generally concluded that the provision of U-anchorage at the end of TRM layers is efficient in preclusion or even delaying the TRM end debonding.
4. A new bond related parameter called "bond-stiffness coefficient (α_b)" was first introduced in this study. This coefficient is the ratio of TRM stiffness to its tensile bond strength. Based on the FE analysis conducted in this study, it is indicated that the TRM composites are effective in enhancing the flexural capacity up to bond-stiffness coefficient of 225, after which both ultimate textile stress and deflection ductility were significantly reduced due to TRM end debonding. Hence, it is recommended for practicing engineers not to design a TRM flexural strengthening scheme with bond-stiffness coefficient more than 225. Otherwise, the effective strain of the textile reinforcement should be limited to the strain level at which debonding may occur. In all cases, the bond-stiffness coefficient should not exceed 290 as the addition of more TRM layers would be ineffective in enhancing the flexural capacity. As long as TRM layers are well anchored at the end and shear failure of beams is precluded, the TRM debonding strain may be conservatively assumed as 70% of the textile rupture strain.
5. Based on the experimental and FE analysis performed in this study, it was observed that TRM-strengthened beams may fail in flexure by either textile rupture or TRM end debonding. The well-known intermediate crack debonding encountered in FRP-strengthened RC beams was not noticed.

References

[1] fib bulletin 14. Externally bonded FRP reinforcement for RC structures. Technical report prepared by the working party EBR of task group 9.3. Lausanne, Switzerland: International Federation for Structural Concrete; 2001.
[2] Triantafillou TC, Papanicolaou CG, Zissimopoulos P, Laourdekis T. Concrete confinement with textile reinforced mortar (TRM) jackets. ACI Struct J 2006;103(1):28–37.
[3] Triantafillou TC, Papanicolaou CG. Shear strengthening of reinforced concrete members with textile reinforced mortar (TRM) jackets. Mater Struct RILEM 2006;39:93–103.
[4] Papanicolaou CG, Triantafillou TC, Bournas DA, Lontou PV. TRM as strengthening and seismic retrofitting material of concrete structures. In: Proc of 1st international conference on textile reinforced concrete (ICTRC). Germany: RWTH Aachen University; 2006. p. 331–40.
[5] Papanicolaou C, Triantafillou T, Papantoniou I, Balioukos C. Strengthening of two-way reinforced concrete slabs with Textile Reinforced Mortars (TRM). In: Proc of the 4th colloquium on textile reinforced structures (CTRS4) und zur 1. Anwendertagung, SFB 528. Eigenverlag: Technische Universität Dresden; 2009. p. 409–20.
[6] Curbach M, Ortlepp R. Besonderheiten des Verbundverhaltens von Verstärkungsschichten aus textilbewehrtem Beton. In: Curbach, M. (Hrsg.), Textile reinforced structures. Proc of the 2nd colloquium on textile reinforced structures (CTRS2), Dresden, Eigenverlag; 2003. p. 361–74 [in German].
[7] Curbach M, Brueckner A. Textile Strukturen zur Querkraftverstaerkung von Stahlbetonbauteilen. In: Curbach, M, editors. Textile reinforced structures. Proc of the 2nd colloquium on textile reinforced structures (CTRS2), Dresden; 2003. P. 347–60 (in German).
[8] Larbi AS, Contamine R, Ferrier E, Hamelin P. Shear strengthening of RC beams with textile reinforced concrete (TRC) plate. Construct Build Mater 2010;24:1928–36.
[9] Bruckner A, Ortlepp R, Curbach M. Anchoring of shear strengthening for T-beams made of textile reinforced concrete (TRC). Mater Struct RILEM 2008;41:407–18.

[10] Al-Salloum YA, Elsanadedy HM, Alsayed SH, Iqbal RA. Experimental and numerical study for the shear strengthening of RC beams using textile reinforced mortar. J Compos Construct, ASCE 2012;1(January/February).

[11] Livermore Software Technology Corporation (LSTC). LS-DYNA user's keyword manual (nonlinear dynamic analysis of structures in three dimensions), vol. 1. Version 971. Livermore, California: LSTC; 2007.

[12] ASTM. Standard test method for compressive strength of hydraulic cement mortars (using 2-in. or [50-mm] cube specimens). ASTM C109/C109M. West Conshohocken, PA, USA: American Society for Testing and Materials; 2008. http://dx.doi.org/10.1520/C0109_C0109M-08.

[13] ASTM. Method of test for tensile strength of hydraulic cement mortars. ASTM C190. West Conshohocken, PA, USA: American Society for Testing and Materials; 1985.

[14] ASTM. Standard test method for pull-off strength of coatings using portable adhesion testers. ASTM D4541-09e1. West Conshohocken, PA, USA: American Society for Testing and Materials; 2009. http://dx.doi.org/10.1520/D4541-09F01.

[15] Belytschko TB, Tsay CS. Explicit algorithms for non-linear dynamics of shells. J Appl Mech Appl Mech Div, ASME 1981;48:209–31.

[16] Murray YD. User's manual for LS-DYNA concrete material model 159. Report no. FHWA-HRT-05-062. USA: US Department of Transportation, Federal Highway Administration National Transportation Systems Center; 2007.

[17] Murray YD, Abu-Odeh A, Bligh R. Evaluation of concrete material model 159. Report no. FHWA-HRT-05-063. USA: US Department of Transportation, Federal Highway Administration National Transportation Systems Center; 2007.

[18] Chang FK, Chang KY. A progressive damage model for laminated composites containing stress concentration. J Compos Mater 1987;21:834–55.

[19] ACI 318-11. Building code requirements for structural concrete and commentary. Detroit, MI, USA: American Concrete Institute; 2011.

[20] Silfwerbrand J. Shear bond strength in repaired concrete structures. Mater Struct/Matdriaux Construct 2003;36:419–24.

[21] Neale KW, Ebead UA, Abdel Baky HM, Elsayed WE, Godat A. Modelling of debonding phenomena in FRP-strengthened concrete beams and slabs. In: Proc of the international symposium on bond behaviour of FRP in structures; 2005. p. 45–54.

[22] ACI Committee 440. Guide for the design and construction of externally bonded FRP systems for strengthening concrete structures. ACI 440.2R-08, Detroit, MI, USA: American Concrete Institute; 2008.